Article

Electrochemical biosensor using DNA embedded phosphorothioate modified RNA for Mercury Ions determination

HUI WANG, Yang Liu, and Gang Liu

ACS Sens., **Just Accepted Manuscript** • DOI: 10.1021/acssensors.7b00892 • Publication Date (Web): 28 Feb 2018

Electrochemical biosensor using DNA embedded phosphorothioate modified RNA for Mercury Ions determination

Hui Wang [a, *], Yang Liu[b] and Gang Liu [a, *]

a. Key Laboratory of Modern Precision Agriculture System Integration Research, Ministry of Education and Key Laboratory of Agricultural Information Acquisition Technology, Ministry of Agriculture, China Agricultural University, Beijing 100083, P.R. China.

b. Xi'an Jiaotong University, School of Electronic and Information Engineering, Xi'an 710049, P.R. China.

Keywords: Mercury, DNA/RNA; Field effect transistor; Single-walled carbon nanotube; Biosensor

Supporting Information Placeholder

ABSTRACT: Mercury (Hg) and its compounds, originating from a variety of nature and anthropogenic source, are ubiquitous in the natural environment, which cause severe environmental contamination and pose irreversible harm to human health. Fast and accurate sensing approach is of significant importance for mercury detection. Here, a label-free biosensor using Hg(II)-induced cleavage of phosphorothioate (PS) modified RNA was exploited. We designed a specific single-stranded DNA embedded four PS-modified RNA (Hg-DPR) to improve the cleavage reaction yield, and then Hg-DPR was covalently linked with single-walled carbon nanotube field effect transistor (SWNTs/FET) via a peptide bond. The Hg-DPR can be efficiently cleaved after exposed to Hg(II), which further causes the conductivity of the SWNTs to change. Using the relative resistance change, the Hg-DPR /SWNTs/FET successfully obtained detection of Hg(II) as low as 10 pM, and the calibration curves were linear in the range of 50 pM to 100 nM and 100 nM to 10 μM. Additionally, DPR/SWNTs/FET exhibited excellent sensitivity, portability and low-cost for Hg(II) detection.

Mercury and its compounds are distributed ubiquitously in the environment, but have high toxicity for organisms even at low concentration[1, 2]. They are emitted to the atmosphere by natural and human sources[3]. The total amount of mercury, originating from degassing of earth's crust, reaches 10,000 tons[4]. As a result of various anthropogenic activities including coal combustion, metal refining, gold and silver extraction, and a variety of industrial[5], the emission of mercury pollutions are increasing approximately 2000 metric tons per year[6]. Fossil fuel combustion and mining are two of the primary pollution sources. Based on statistics and analysis, the burning coal can release about 395 ng/g of mercury to surrounding environment. In the US, it emits around 33 tons of mercury pollution every year. Refining gold from amalgam in gold

mining is the second largest pollution source. Every year, 10 to 20 millions of gold miners are burned in the world, and each gram of amalgam burning releases 1.2-1.5 mg of mercury to the environment[7].

Mercury has three forms (elemental, inorganic mercury and the organic ones) in natural[8]. The elemental form is removed from the atmosphere after oxidation to Hg(II), and then deposited to land and ocean[3]. Hg(II), an inorganic form, can cause severe adverse effects on human health, and it also can be transformed into lipophilic organic compound, methylmercury, by reducing sulfate aquatic bacteria[9]. These two forms are easily absorbed by animals and plants with bioaccumulation occurring at higher trophic levels of the food chain. People with high dietary intake these contaminated food, which will absorb by the gastrointestinal tract, and accumulated to different human tissues[10]. If the level of mercury in organs exceeds the normal limit, it's toxicity will cause long-term adverse effects on biological systems such as nervous, renal, motor, immune, and reproductive system.The symptoms of health problems include memory deficit, increased fatigue, decreased muscular strength, plasma creatinine level brain damage, kidney failure, and various motion disorders[11, 12]. To ensure the environment and food safety, the US Environmental Protection Agency (EPA) sets the maximum allowable mercury level in drinking water at 10 nM, and the China Food and Drug Administration requires the total mercury level in grain and vegetable below to 0.02 mg/kg and 0.01 mg/kg, respectively.

Rapid and accurate determining the concentration of mercury is an increasing demand to evaluate environment and food safety. To date, the rountine analytical techniques for Hg(II) detection including atomic absorption spectroscopy (AAS) [13], cold-vapor atomic fluorescence spectrometry (CV/AFS) [14, 15], cold-vapor atomic absorption spectroscopy (CV/AAS)[16] , inductively coupled plasma atomic emission spectrometry (ICP/AES)[17], high performance liquid chromatography-cold-vapor-inductively coupled plasma mass spectrometry (HPLC/CV/ICP/MS)[18] and inductively coupled plasma mass spectrometry (ICP/MS)[19] have been developed, and widely used in food and environmental testing laboratories and agencies. These methods have high selectivity and sensitivity, however, the commercial devices are bulky and expensive, and require time-consuming sample preparation processes and well-trained professional operators, which are difficult to test the Hg(II) on-site.

Various new techniques have been exploited to overcome these problems. Electrochemical technique has been demonstrated as a powerful and effective method, which just need a tiny electronic device transforming chemical signal to electronic signal. Moreover, newly developed nanomaterials and biomaterials (organic molecules, peptides, lipids, proteins, and oligonucleotides) [20, 21] provide tremendous potential to improve the characteristics of detecting sensors. Biosensors based on protein enzyme inhibition show fast, high sensitivity and selectivity for Hg(II) detection, but the unstable activity of enzyme and ribozymes in the ambient environment limits application, especially in the field. Over the past two decades, DNA molecules known as DNA and DNAzyme[22] have emerged and offered a very useful material for metal sensing. They

own high specificity and affinity with cofactors, such as Na(I)[23], Ag(I)[24], Pb(II)[25], Cu(II)[26], Mg(II)[27], Ca(II)[28], Zn(II)[29], Cd(II)[30], Mn(II), UO_2(II)[31], and Hg(II). Different from protein enzymes, DNA molecules can be denatured and renatured many times without losing their binding ability or activity toward substrates. DNA molecules for Hg(II) detection are mainly based on "T-Hg-T" interactions[32]. By comparison, DNAzymes are more convenient and effective because they cost less to produce and are more resistant to hydrolysis. Some groups have reported RNA-cleaving DNAzymes for Hg(II) detection, but these sensors need two steps: (1) Hg(II) bind with T base to form a herin structure, (2) the biosensor requires UO_2(II) to catalyze the DNAzyme. Although both DNA and DNAzyme are very sensitive and selective to Hg(II), they need a long time due to the binding process of "T-Hg-T", or occur mismatches and no hybridization. Recently, Liu and coauthors found that a single phosphorothioate-modified RNA[33]. DNA chimeric substrate is unique to Hg(II) among the various divalent metal ions that can be cleaved efficiently by Hg(II), which provides a new mechanism for Hg(II) detection.

Single-walled carbon nanotubes (SWNTs)[34] is a one-dimensional structure of semiconductor nanomaterials, which has outstanding electronic, chemical, mechanical, thermal, and optical properties. Field-effect transistor (FET) coupling with SWNTs shows a lot of potential in low-concentration and real-time detection. Here, a new biorecognition 'Hg-DPR' using a single-stranded DAN embedded four Hg(II)-induced cleavage of phosphorothioate modified RNA was designed, which has highly selective for Hg. We also developed a label-free, facile, and low-cost biosensor integrated 'Hg-DPR' with an extremely sensitive SWNTs-FET to enable detection of the extremely low concentration. The mechanism is that Hg-DPR cleaved by Hg(II) results in a change in conductance of the SWNTs, and the cleaved efficiency in direct proportion to Hg(II) concentration. This is the first report of a biosensor using Hg-induced cleavage of PS-modified RNA and SWNTs-FET combination for electronic detection of Hg(II).

2. Materials and methods

2.1. Chemicals and materials

DNA sequences with or without phosphorothioate(PS) -modified RNA were purchased from Shanghai Sangon Biological Engineering Technology & Services Co. Ltd. (Shanghai, China), which are synthesized and purified using standard solid phase techniques. The DNA sequences are listed below.

Hg-DNA: /5AmMC6/ GAGCGAATAGAAGAAAACGGCGGAAACGCCGAACGCTC

Hg-RNA: /5AmMC6/GrAGrCGAATrAGArAGAAAACGGCGGAAACGCCGAACGCTC

Hg-DPR : /5AmMC6/GrA*GrC*GAATrA*GArA*GAAAACGGCGGAAACGCCGAACGCTC

Semiconducting single-walled carbon nanotubes (95%, 0.01 mg/mL) was bought from Nano-Integris Inc. (USA). Metal salts including $Cu(NO_3)_2$, $Mg(NO_3)_2$, $Hg(NO_3)_2$, $CaCl_2$, $Mn(NO_3)_2$, $Zn(NO_3)_2$, $Cr(NO_3)_3$, $Pb(NO_3)_2$, $Ni(NO_3)_2$, $Fe(NO_3)_3$, $Co(NO_3)_2$ and $Cd(NO_3)_2$ were purchased from Sigma Aldrich (USA). 1-Pyrenebutanoic acid succinimidyl ester (PBASE), N, N-dimethylformamide (DMF, anhydrous, 99.8%), 6-mercapto-1-hexanol (MCH, 97%), and ethanolamine were also offered by Sigma Aldrich (USA). 2-(N-morpholino) ethanesulfonic acid (MES), 3-(N-morpholino) propanesulfonic acid (MOPS) and sodium hydroxide were obtained from Mandel Scientific Inc. 3-Aminopropyltriethoxysilane (APTES, 99%) and ethanolamine (EA, 99%) was offered by Acros Organics. Tween 20 was bought from Bio-Rad. All of the chemical reagents were of analytical grade and used without further purification. All the stock and buffer solutions were prepared using ultrapure water generated from a Millipore Milli-Q water purification system (Billerica, MA, USA) with an electric resistance of 18.2 MΩ, and treated through high-temperature sterilization. The Hg-DPR solution (100 μM) was prepared in 20 mM MOPS buffer (pH 7.4).

2.2. Apparatus

All characteristics of the Hg-DPR/SWNTs/FET were measured using a Keithley 2636 precision semiconductor parameter analyzer at room temperature. For voltage-current (I_{DS}-V_{DS}) measurement, the voltage between drain and source was sweeping from -0.2 V to 0.2 V in steps of 0.01 V, and the gate voltage was 0 V (V_{GS}=0 V). SEM images were obtained with a Zeiss Leo SUPRA 55 at acceleration voltage at 10 KV. Raman spectra were recorded using Dilor XY Laser Raman with imaging microscope (514 nm Diode and Ar ion lasers). UV spectrum was collected by Beckman DU800 UV/Vis spectrophotometer (Beckman Coulter, Inc. USA).

2.3 Fabrication of SWNTs/FET

The interdigital electrode was microfabricated on a high doped p-type silicon wafer with 100 nm thick thermal oxide (SiO_2) using standard lithographic patterning. The silicon wafer was covered with a uniform film of photoresist and written interdigital structure through photolithographically defining the electrode area. After baking and cleaning, 20 nm-thick chrome adhesion film and 180 nm-thick gold layer were deposited on the surface via e-beam. Finally, the deposited wafer was immersed in acetone for overnight to remove the unwritten parts.

The SWNTs devices were fabricated through following the steps reported by Ramnani et al. First, the chip was rinsed successively with acetone, isopropanol, and ammonium hydroxide to clean up surface residues. Second, the cleaned device was immersed in APTES, incubated for 30 min, and then rinsed with sufficient Milli-Q water. Third, SWNTs solution were

dispersed onto a SiO_2/Si substrate through the spray method with high humidity conditions for 60 min, followed by washing the SWNTs residue and annealing in air at 250 °C.

2.4 Hg-DPR Immobilization

To functionalize Hgzyme, SWNTs/FET was treated using the protocol shown in Fig.1. First, SWNTs/FET was immersed in 10 mM MCH for 30 min to block the gold surface, and tread with a 6 mM PBASE in dimethylformamide for 60 min at room temperature followed by being rinsed with DMF and Milli-Q water to eliminate the unbonded PBASE. Next, the processed electrode was incubated in 100 μM Hg-DPR at 4 °C for overnight to make the amine at the 5' end of Hg-DPR bind with ester group of PBASE, which the mfold was shown in Fig. S1. The excess ester groups of PBASE were blocked with 0.1 mM EA, and the surface of SWNTs was blocked using 0.1% Tween 20 to prevent non-specific binding to SWNTs.

2.5 Sensing protocol

To measure Hg(II) concentration, 20 μL of the tested solution was dropped and covered on Hg-DPR/SWNTs/FET's surface for 3 min, and then rinsed with sufficient EOPS buffer solution for several times to remove Hg(II) residues. Finally, the Hg-DPR/SWNTs/FET was covered with 20 μL EOPS buffer solution (pH 7.4), and collected the current-voltage.

The relative resistance of Hg-DPR/SWNTs/FET was defined as the following equation:

$$\triangle R/R = (R_0 - R)/R_0 \times 100\%$$

Where R_0 was the resistance before Hg-DPR/SWNTs/FET exposure to Hg(II) solution, and R is the resistance after explored to Hg(II) solution.

3. Results and Discussion

3.1. Characterization

Fig. 2(A) shows the microstructure of interdigital electrode, which has ten pairs of interdigital finger. The gap between fingers was 3 μm, and the length and width of each finger were 200 μm and 5 μm in Fig. 2(B), respectively. The SEM and Raman were employed to study FET before and after functionalized with SWNTs. SEM image in Fig 2(C) exhibits the high-density of SWNTs network that was uniformly dispersed on the FET surface.

Fig. 3(A) shows the Raman spectrum of FET before and after functionalized with SWNTs using 514 nm laser excitation. There was no peak on the blank FET (black curve) during 100 cm^{-1} to 300 cm^{-1} and 1200 cm^{-1} to 3500 cm^{-1}. After SWNTs was modified on FET via APTES, several bands were located at 178 cm^{-1}, 1345 cm^{-1}, 1592 cm^{-1} and 2682 cm^{-1}. According to the literature, these bands were consistent with RBM-band, D-band, G-band and G'-band of the Raman spectrum of SWNTs. SEM and Raman demonstrated the SWNTs attached to FET are stable and tight. Fig. 3(B) shows the UV-vis absorption spectra of quartz subtract functionalized with SWNTs, PBASE, Hg-DPR, EA and TWEEN 20 ranging from 200 nm to 600 nm. Here, we used blank quartz to replace silicon substance due to the excellent optical transmittance of quartz. Compared with blank quartz, the absorbance intensity of SWNTs/Quartz improved during the whole spectra rang, and an absorption peak was found at 260 nm, illustrating SWNTs was immobilized on the quartz surface[35, 36]. There were three absorbance peaks discovered after SWNTs/Quartz incubated in PBASE, which indicated pyrene ring had attached on the SWNTs surface through the π–π interaction. This phenomenon was consistent with the previously reported article[37]. When SWNTs-PBASE functionalized with Hg-DPR, only one absorption peak was observed at 275 nm, which might be all of the peaks overlapped with DNA to generate a composite effect.

Fig.4 shows the I_{DS}-V_{DS} of SWNTs functionalized with MCH, PBASE, Hg-DPR, EA and Tween20. It was clear that I_{DS} continued to decrease after each modified step, which demonstrated these chemical reagent and material had bonded with SWNTs/FET and affected the resistance of SWNTs. After MCH modification, the resistance almost no change because the sulphydryl of MCH only bound with Au through Au-S bonds, and form a nonconductive membrane. PBASE was attached with SWNTs surface through π–π interaction between SWNTs and pyrene. Hg-DPR was immobilized with PBASE-modified SWNT covalently via an amide bond between the amine at the 5′ end and the ester groups of PBASE. EA was used to block the unbind PBASE, and Tween20 prevented non-specific binding to SWNTs, resulting in a decrease of the charge carrier concentration of the p-type SWNTs and electron scattering from these molecules.

3.2. Optimization

To simplify detection processes and obtain excellent analytical performance, some parameters were optimized through detecting different Hg(II) concentrations.

To illustrate the cleavage site of Hg-DPR, we first investigated the DNA with and without embedded different types of RNA in Fig.5 (A). The relative resistances of Hg-DNA/SWNTs/FET did not change before and after exposure to three Hg(II) concentrations. When some DNA bases were replaced by RNA bases without PS modification, the relative resistances of Hg-RNA/SWNTs/FET were still no change in the presence of different Hg(II) concentrations. However, after DNA with

four PS-modified RNA, the relative resistances of Hg-DPR/SWNTs/FET for different Hg(II) concentrations changed significantly. The reason was probably that Hg(II) had strong thiophilicity[33]. The charge of the sulfur was neutralized after Hg(II) bond with the sulfur atom, which can make it a better leaving group in the nucleophilic attack by the 2'-OH group of the ribo-adenosine. Therefore, it demonstrated this Hg(II)-cleavage occurs the position of PS-modified RNA.

Fig.S2 shows the voltage-current curves for the detection of different Hg(II) concentrations (0, 1 nM, 100 nM and 10 μM). The relationship between current and voltage ranging from -0.2 V to 0.2 V exhibited nonlinearity. By using Ohm's law, we found the resistance values in Fig.S3 were decreasing along with the voltage increasing between the source and the drain, excluding 0 V. The reason might be ascribed to the semiconducting property of SWNTs, which will be affected by alkaline buffer solution approximately equated to a negative base voltage. However, the relative resistances at different voltage were almost the same value in Fig.5(B). Based on the energy saving and stability, 0.02 V was chosen to simplify detection process in the following experiment.

Fig.5(C) shows the relative resistance of Hg-DPR/SWNTs/FET for Hg detection effected by pH value. The cleavage reaction of PS-modified RNA had a similar amount of product from pH 5.5 to 7.0. However, the relative resistances are of positive relevance with the pH values in the range from 6.0 to 7.0, which were contributed to the hydrogen ions in the solution. The prone of SWNTs were easily accepted by the H(I), it needed a long time to recover after we add 7.4 buffer solution. The relative resistance showed opposite correlation with pH value if pH >7.0 that might be Hg(II) hydrolysis at higher pH. Therefore, a pH of 7.0 was found to be suitable for the experiment.

Fig.5(D) shows the relationship between relative resistance and incubation time in the range from 0 to 4 min. Thee different Hg(II) concentrations (100 pM, 10 nM and 1uM) were selected for further study. Hg-DPR/SWNTs/FET was immersed to a certain Hg(II) concentration, and recorded the resistance change every 30 s. We found that reaction time of Hg(II) cleaved PS-modified RNA were proportional to Hg(II) concentrations. The reaction time of Hg-DPR/SWNTs/FET needed 60 s, 90 s and 120 s for these three different Hg(II) concentrations, respectively. To make sure the stability of reaction, 3 min was chosen for the experiment.

3.3. Sensitivity for Hg(II) detection

Under the optimum conditions analyzed above, the analytical performance of Hg-DPR/SWNTs/FET were investigated by monitoring the relative resistance change with different Hg(II) concentrations. As shown in Fig. 6A, in the absence of Hg(II) concentration, the relative resistance was very low, indicating DNA embedded PS-modified RNA was not cleaved. After exposed to Hg(II) concentration, the relative resistance increased gradually in the low concentration range, and continued to

rise sharply in high concentration range. The relative resistance revealed excellent relationship with the logarithm of Hg(II) concentration in the range of 50 pM to 100 nM and 100 nM to 10 μM. The regression equations were y_1=5.461x+0.957 and y_2=32.313x-135.67 with the linear regression correlation coefficient of 0.990 and 0.991, respectively. The detection limit of Hg(II) was 10 pM(S/N =3), which is significantly below the allowable mercury level (10 nM) in drinkable water required by the United States Environmental Protection Agency (USEPA), and also satisfied the China Food and Drug Administration.

Tab. 1 presents some parameters of other published sensors including the linear range, limit of detection and testing time. It illustrated that Hg-DPR/SWNTs/FET own a wide linear range and lower limit of detection than other published sensors. Even though the testing time was longer than parts of sensors, 3 min for one measurement was a relatively short period of time, and acceptable for rapid Hg(II) determination.

3.4 Interference

To evaluate the selectivity, Hg-DPR/SWNTs/FET was used to measure and compare the relative resistance of Hg(II) before and after adding other metal ions CH_3Hg, K(I), Li(I), Na(I), Ni(I), Mg(II), Pb(II), Cd(II), Zn(II), Cu(II), Bi(III), Fe(III) and Cr(III), which probably existed in real water and soil sample. Under the optimized conditions, Hgzyme/SWNTs/FET in the presence of 1 μM Hg(II) could induce a significant enhancement of relative resistance. After adding other metal ions at the same concentration of Hg(II), nearly all of the relative resistance changed imperceptibly. Therefore, the proposed biosensor had high selectivity to discriminate Hg(II) from others.

3.6 Real sample analysis

To evaluate the practical application, we used the Hg-DPR/SWNTs/FET to measure the concentrations of Hg(II) in soil and pond water samples. Water and soil samples collected from lake and farmland in the suburbs of Beijing. The water samples were filtered through a 0.22 μm membrane to remove large particles and solid insoluble substances. Soil samples were collected from a local field in Beijing and pretreated using the following steps. Preliminary, soil samples were dried naturally and then ground into small particles using the Grinding machine. Weighing 2 g soil was mixed with 0.1 M nitric acid, and sonicated for 60 min. Additionally, the mixture solution was centrifuged and filtered by a 0.45 μm membrane. Finally, the filtered solutions were adjusted to pH 7.0.

Water samples and soil extracting solution were also detected by a standard method of Atomic fluorescence spectrometer analysis method (AFS). The results using the two methods were shown in Tab. 2. The detecting values were quite close, and

the relative errors were below 10%. To assess the accuracy of Hg-DPR/SWNTs/FET, a t-test was used to analyze these results of two methods. After calculation, we got P= 0.963> 0.05, suggesting the two methods did not significantly different. All these can demonstrate that the proposed biosensor is applicable for Hg(II) detection in real samples.

4. Conclusion

In conclusion, we designed a new type structure of Hg-DPR with four embedded Hg-induced cleavage of PS-modified RNA, which made the cleavage reaction yield 50%. The Hg-DPR was bond with SWNTs based FET platform via peptide linkage, which offered a simple biosensor for Hg(II) detection. The Hg(II) can cleave Hg-DPR with fast rate, which led to a structural switch in a short time and further affected the conductivity of SWNTs. Hg-DPR /SWNTs/FET shown excellent sensitivity and selectivity for sensing Hg(II) with a lower limit of detection down to 10 nM, which was lower than the maximal allowable Hg(II) level defined by the USEPA. Compared with standard optical methods, the simple, portable and easy-to-use device offered a promising potential for on-site detecting Hg(II).

ASSOCIATED CONTENT

Supporting Information

The Supporting Information is available free of charge.

The mfold of Hg-DPR, the current-voltage and resistance of Hg-DPR/SWNTs/FET with the different Hg(II) concentrations (PDF).

AUTHOR INFORMATION

Corresponding Author

Gang Liu, Professor., Research interests: Electrochemical sensor and biosensor, Image Sensor and Tractor navigation. Tel/Fax: +86-010-62736741; Email: pac@cau.edu.cn.

Hui Wang, Ph.D., Research interests: Electrochemical sensor and biosensor for heavy metal ions and VOCs detection. Email: wanghui_lunwen@163.com.

Present Addresses

17 Qinghua East Road, Haidian District, Beijing, China.

ORCID:

Hui Wang: 0000-0002-0041-5957;

Yang Liu: 0000-0002-4075-1971;

Gang Liu: 0000-0001-9616-9713;

Notes

The authors declare no competing financial interests.

ACKNOWLEDGMENT

This work was supported by Chinese National Natural Science Foundation (No. 31671578), National High Technology Research and Development Program of China (No.2013AA102302).

REFERENCES

(1) Zheng, L.; Liu, G.; Chou, C.-L., The distribution, occurrence and environmental effect of mercury in Chinese coals. *Science of the Total Environment* **2007,** 384, (1), 374-383.

(2) Li, C.; Zhang, Q.; Kang, S.; Liu, Y.; Huang, J.; Liu, X.; Guo, J.; Wang, K.; Cong, Z., Distribution and enrichment of mercury in Tibetan lake waters and their relations with the natural environment. *Environmental Science and Pollution Research* **2015,** 22, (16), 12490-12500.

(3) Lamborg, C. H.; Hammerschmidt, C. R.; Bowman, K. L.; Swarr, G. J.; Munson, K. M.; Ohnemus, D. C.; Lam, P. J.; Heimburger, L. E.; Rijkenberg, M. J.; Saito, M. A., A global ocean inventory of anthropogenic mercury based on water column measurements. *Nature* **2014,** 512, (7512), 65-68.

(4) Zahir, F.; Haq, R. S. K.; Khan, R. H., Low dose mercury toxicity and human health. *Environmental Toxicology & Pharmacology* **2005,** 20, (2), 351-360.

(5) Simone, F. D.; Gencarelli, C. N.; Hedgecock, I. M.; Pirrone, N., A Modeling Comparison of Mercury Deposition from Current Anthropogenic Mercury Emission Inventories. *Environmental science & technology* **2016,** 50, (10), 5154-5162.

(6) Krabbenhoft, D. P.; Sunderland, E. M., Global change and mercury. *Science* **2013,** 341, (6153), 1457-1458.

(7) Jiang, G. B.; Shi, J. B.; Feng, X. B., Mercury Pollution in China. *Environmental science & technology* **2006,** 40, (12), 3672-3678.

(8) Rebelo, F. M.; Caldas, E. D., Arsenic, lead, mercury and cadmium: Toxicity, levels in breast milk and the risks for breastfed infants. *Environmental research* **2016,** 151, 671-688.

(9) Farina, M.; Avila, D. S.; Rocha, J. B. T. D.; Aschner, M., Metals, Oxidative Stress and Neurodegeneration: A focus on Iron, Manganese and Mercury. *Neurochemistry international* **2013,** 62, (5), 575-594.

(10) Rebelo, F. M.; Caldas, E. D., Arsenic, lead, mercury and cadmium: Toxicity, levels in breast milk and the risks for breastfed infants. *Environmental research* **2016,** 151, 671-688.

(11) Ou, L.; Chen, C.; Chen, L.; Wang, H.; Yang, T.; Xie, H.; Tong, Y.; Hu, D.; Zhang, W.; Wang, X., Low-Level Prenatal Mercury Exposure in North China: An Exploratory Study of Anthropometric Effects. *Environmental science & technology* **2015,** 49, (11), 6899-6908.

(12) Buck, K. A.; Varian-Ramos, C. W.; Cristol, D. A.; Swaddle, J. P., Blood Mercury Levels of Zebra Finches Are Heritable: Implications for the Evolution of Mercury Resistance. *PloS one* **2016,** 11, (9), 1-14.

(13) Bagheri, H.; Naderi, M., Immersed single-drop microextraction-electrothermal vaporization atomic absorption spectroscopy for the trace determination of mercury in water samples. *J Hazard Mater* **2009,** 165, (1-3), 353-358.

(14) da Silva, M. J.; Paim, A. P.; Pimentel, M. F.; Cervera, M. L.; de la Guardia, M., Determination of mercury in rice by cold vapor atomic fluorescence spectrometry after microwave-assisted digestion. *Analytica chimica acta* **2010,** 667, (1-2), 43-48.

(15) Yuan, C.-G.; Lin, K.; Chang, A., Determination of trace mercury in environmental samples by cold vapor atomic fluorescence spectrometry after cloud point extraction. *Microchimica Acta* **2010,** 171, (3-4), 313-319.

(16) Pourreza, N.; Ghanemi, K., Determination of mercury in water and fish samples by cold vapor atomic absorption spectrometry after solid phase extraction on agar modified with 2-mercaptobenzimidazole. *J Hazard Mater* **2009,** 161, (2–3), 982-987.

(17) Zhu, X.; Alexandratos, S. D., Determination of trace levels of mercury in aqueous solutions by inductively coupled plasma atomic emission spectrometry: Elimination of the 'memory effect'. *Microchemical Journal* **2007,** 86, (1), 37-41.

(18) de Souza, S. S.; Campiglia, A. D.; Barbosa, F., Jr., A simple method for methylmercury, inorganic mercury and ethylmercury determination in plasma samples by high performance liquid chromatography-cold-vapor-inductively coupled plasma mass spectrometry. *Analytica chimica acta* **2013,** 761, 11-17.

(19) Bushee, D. S., Speciation of mercury using liquid chromatography with detection by inductively coupled plasma mass spectrometry. *The Analyst* **1988,** 113, (8), 1167-1170.

(20) Zhou, W.; Yu, T.; Vazin, M.; Ding, J.; Liu, J., Cr^{3+} Binding to DNA Backbone Phosphate and Bases: Slow Ligand Exchange Rates and Metal Hydrolysis. *Inorganic chemistry* **2016,** 55, (16), 8193-8200.

(21) Zaib, M.; Athar, M. M.; Saeed, A.; Farooq, U., Electrochemical determination of inorganic mercury and arsenic--A review. *Biosensors & bioelectronics* **2015,** 74, 895-908.

(22) Zhou, W.; Saran, R.; Liu, J., Metal Sensing by DNA. *Chem Rev* **2017,** 117, (12), 8272-8325.

(23) Zhou, W.; Ding, J.; Liu, J., A highly specific sodium aptamer probed by 2-aminopurine for robust Na^{+} sensing. *Nucleic acids research* **2016,** 44, (21), 10377-10385.

(24) Saran, R.; Kleinke, K.; Zhou, W.; Yu, T.; Liu, J., A Silver-Specific DNAzyme with a New Silver Aptamer and Salt-Promoted Activity. *Biochemistry* **2017,** 56, (14), 1955-1962.

(25) Saran, R.; Liu, J., A comparison of two classic Pb^{2+}-dependent RNA-cleaving DNAzymes. *Inorganic Chemistry Frontiers* **2016,** 3, (4), 494-501.

(26) Huang, P.-J. J.; Liu, J., An ultrasensitive light-up Cu^{2+} biosensor using a new DNAzyme cleaving a phosphorothioate-modified substrate. *Analytical chemistry* **2016,** 88, (6), 3341-3347.

(27) Gao, X.; Huang, H.; Niu, S.; Ye, H.; Lin, Z.; Qiu, B.; Chen, G., Determination of magnesium ion in serum samples by a DNAzyme-based electrochemical biosensor. *Analytical Methods* **2012,** 4, (4), 947-952.

(28) Zhou, W.; Saran, R.; Huang, P. J. J.; Ding, J.; Liu, J., An Exceptionally Selective DNA Cooperatively Binding Two Ca2+ Ions. *ChemBioChem* **2017,** 18, (6), 518-522.

(29) Kong, R.-M.; Fu, T.; Sun, N.-N.; Qu, F.-L.; Zhang, S.-F.; Zhang, X.-B., Pyrophosphate-regulated Zn^{2+}-dependent DNAzyme activity: An amplified fluorescence sensing strategy for alkaline phosphatase. *Biosensors and Bioelectronics* **2013,** 50, 351-355.

(30) Huang, P.-J. J.; Liu, J., Rational evolution of Cd2+-specific DNAzymes with phosphorothioate modified cleavage junction and Cd^{2+} sensing. *Nucleic acids research* **2015,** 43, (12), 6125-6133.

(31) Lee, J. H.; Wang, Z.; Liu, J.; Lu, Y., Highly sensitive and selective colorimetric sensors for uranyl (UO_2^{2+}): Development and comparison of labeled and label-free DNAzyme-gold nanoparticle systems. *Journal of the American Chemical Society* **2008,** 130, (43), 14217-14226.

(32) Huang, P.-J. J.; van Ballegooie, C.; Liu, J., Hg^{2+} detection using a phosphorothioate RNA probe adsorbed on graphene oxide and a comparison with thymine-rich DNA. *The Analyst* **2016,** 141, (12), 3788-3793.

(33) Huang, P. J. J.; Wang, F.; Liu, J., Cleavable Molecular Beacon for Hg^{2+} Detection Based on Phosphorothioate RNA Modifications. *Analytical chemistry* **2015,** 87, (13), 6890.

(34) Peng, G.; Wu, S.; Ellis, J. E.; Xu, X.; Xu, G.; Yu, C.; Star, A., Single-walled carbon nanotubes templated CuO networks for gas sensing. *J. Mater. Chem. C* **2016,** 4, (27), 6575-6580.

(35) Moraes, R. A.; Matos, C. F.; Castro, E. G.; Schreiner, W. H.; Oliveira, M. M.; Zarbin, A. J., The effect of different chemical treatments on the structure and stability of aqueous dispersion of iron-and iron oxide-filled multi-walled carbon nanotubes. *Journal of the Brazilian Chemical Society* **2011,** 22, (11), 2191-2201.

(36) Shi, Y.; Ren, L.; Li, D.; Gao, H.; Yang, B., Optimization conditions for single-walled carbon nanotubes dispersion. *Journal of Surface Engineered Materials and Advanced Technology* **2013,** 3, (01), 6.

(37) Prakash, R.; Superfine, R.; Washburn, S.; Falvo, M. R., Functionalization of carbon nanotubes with proteins and quantum dots in aqueous buffer solutions. *Applied physics letters* **2006,** 88, (6), 063102.

(38) Jiang, S.; Cheng, R.; Ng, R.; Huang, Y.; Duan, X., Highly sensitive detection of mercury(II) ions with few-layer molybdenum disulfide. *Nano Research* **2015,** 8, (1), 257-262.

(39) Sener, G.; Uzun, L.; Denizli, A., Lysine-Promoted Colorimetric Response of Gold Nanoparticles: A Simple Assay for Ultrasensitive Mercury(II) Detection. *Analytical chemistry* **2014,** 86, (1), 514-520.

(40) Wang, W.; Kang, T. S.; Wai, P.; Chan, H.; Lu, J. J.; Chen, X. P.; Leung, C. H.; Ma, D. L., A label-free G-quadruplex-based mercury detection assay employing the exonuclease III-mediated cleavage of T–Hg^{2+}–T mismatched DNA. *Science & Technology of Advanced Materials* **2015,** 16, (6), 065004.

(41) Chen, K.; Lu, G.; Chang, J.; Mao, S.; Yu, K.; Cui, S.; Chen, J., Hg(II) ion detection using thermally reduced graphene oxide decorated with functionalized gold nanoparticles. *Analytical chemistry* **2012,** 84, (9), 4057.

(42) Ren, W.; Zhang, Y.; Huang, W. T.; Li, N. B.; Luo, H. Q., Label-free colorimetric detection of Hg^{2+} based on Hg^{2+} -triggered exonuclease III-assisted target recycling and DNAzyme amplification. *Biosensors & bioelectronics* **2015,** 68, 266.

(43) Dr, J. L.; Yi, L. P., Rational Design of "Turn-On" Allosteric DNAzyme Catalytic Beacons for Aqueous Mercury Ions with Ultrahigh Sensitivity and Selectivity †. *Angewandte Chemie* **2007,** 119, (40), 7731–7734.

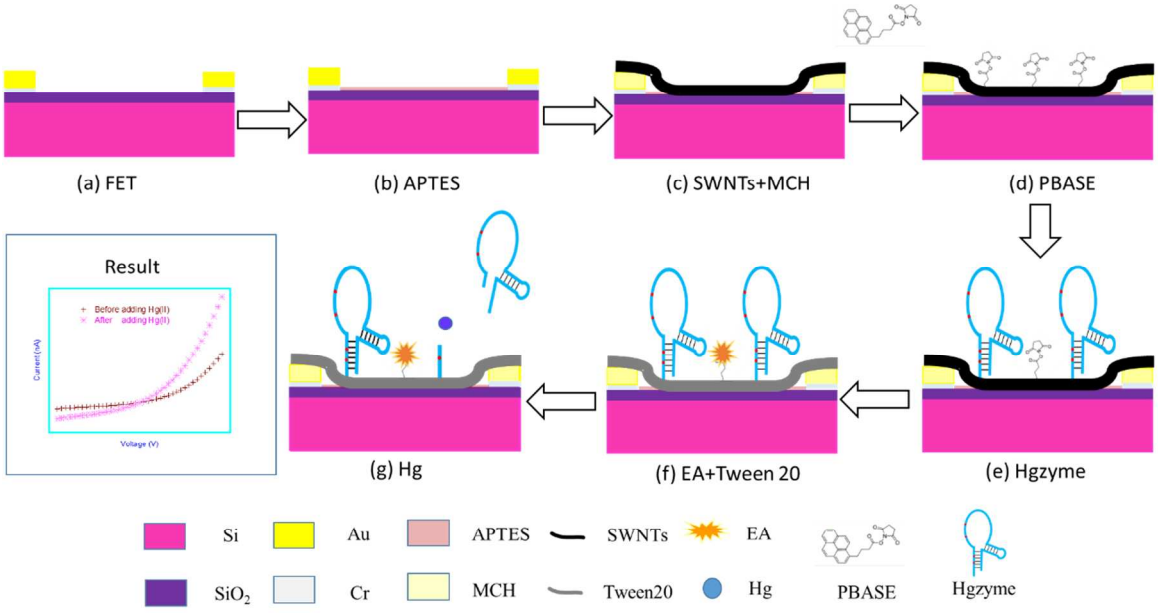

Figure 1. (a-f)Schematic illustration of interdigital electrode functionalized with different materials (FET inclubated in SWNTs, MCH, PBASE, Hg-DPR, EA, and TWEEN20 in successive), and (g) the mechanism of Hg(II) detection (Hg-DPR cleaved by Hg(II)).

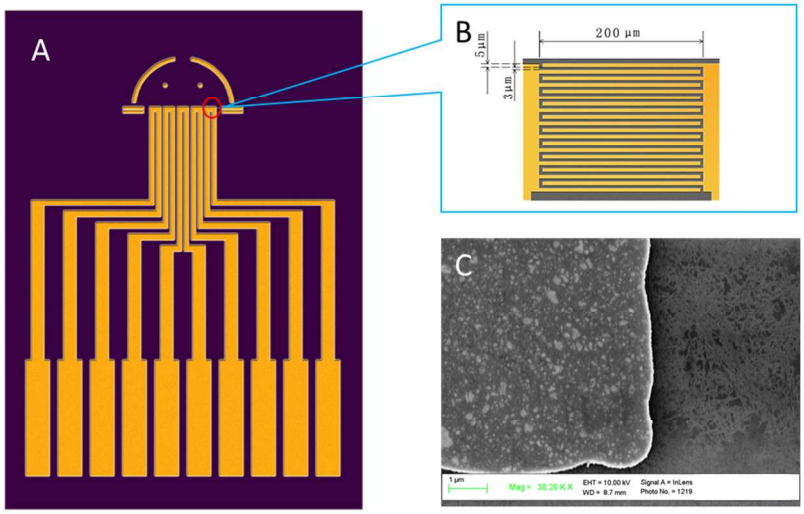

Figure 2. (A) The microscope image of the chip with 5 set of interdigitated electrodes; (B) The microstructure of each interdigital electrode; (C) SEM image of SWNTs networks produced by APTES-assisted assembly technique.

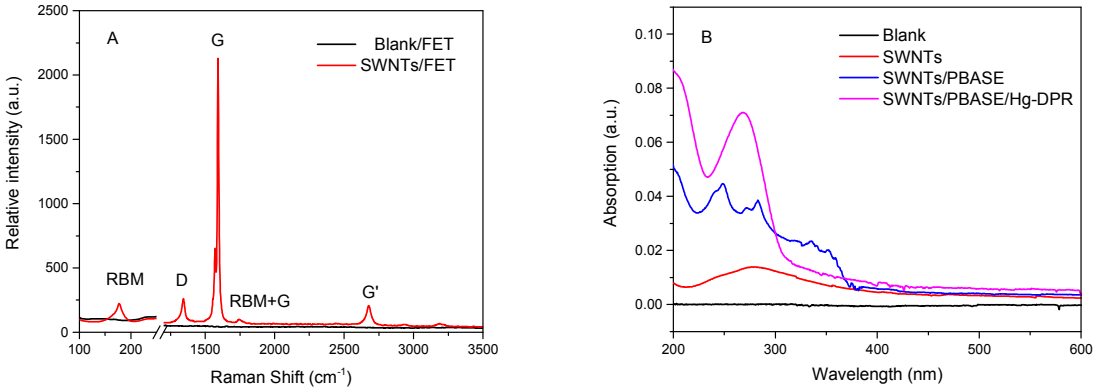

Figure 3 (A) Raman spectra of FET before and after functionalized with SWNTs; (B)UV-vis absorption spectra of quartz subtract functionalized with SWNTs, PBASE, and Hg-DPR.

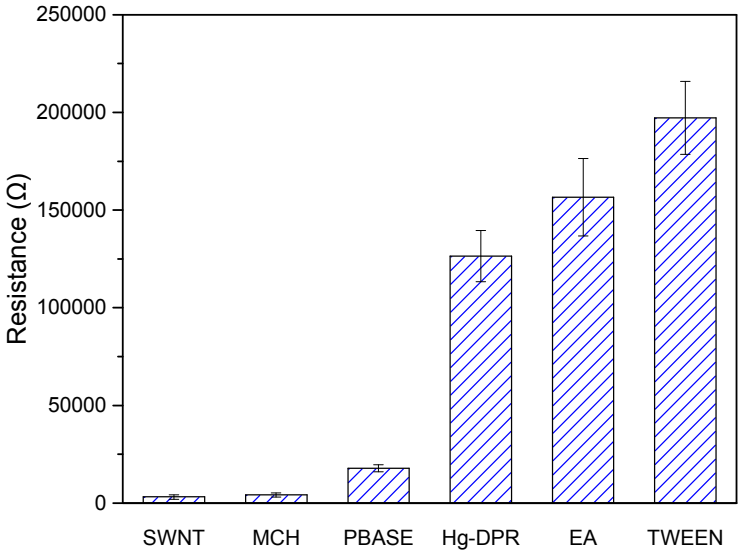

Figure 4. The resistance changes after SWNTs modified MCH, PBASE, Hg-DPR, EA and Tween20 at V_{DS}= 0.2V, V_G=0 V. Each data point is an average of measurements from 5 independent biosensors.

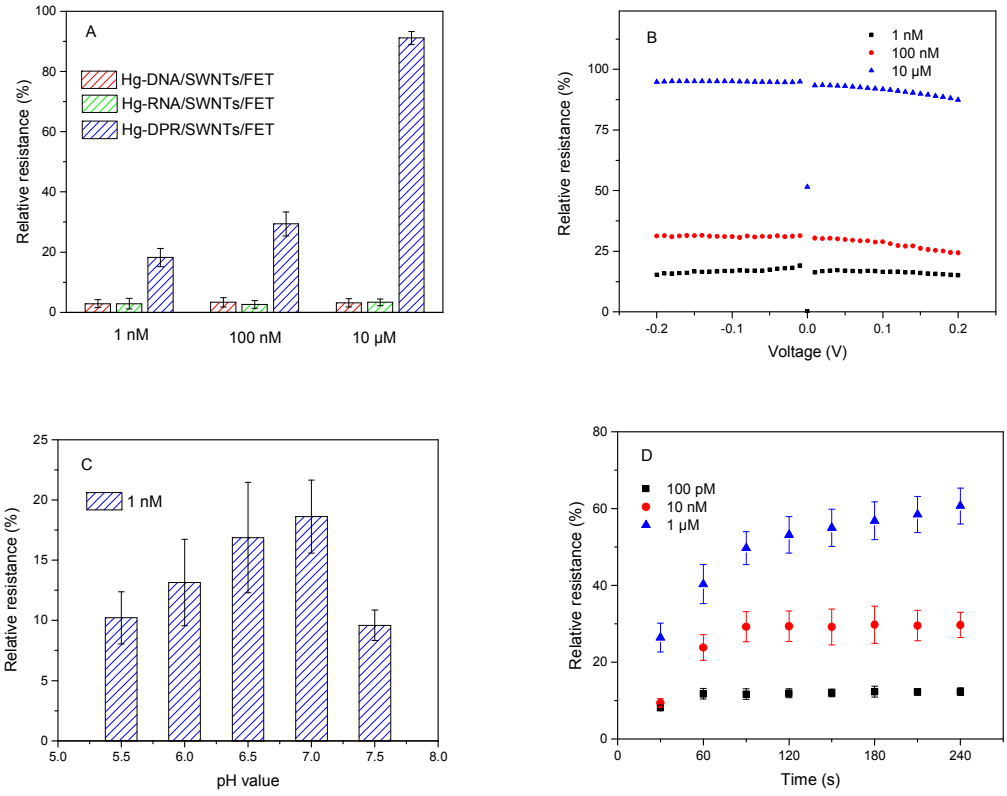

Figure 5. (A) Effect of the base type for three Hg(II) concentrations detection (1nM, 100 nM and 10 μM); (B) the relative resistance effected by V_{DS} ranging from -0.2 V to 0.2 V at V_G=0 V with three Hg(II) concentrations (1 nM, 100 nM and 10 μM); (C) Effect of pH value on the performance of Hgzyme/SWNTs/FET with 1 nM Hg(II) concentration at V_{DS}=0.02 V and V_G=0 V; (D)Effect of incubation time on the performance of Hgzyme/SWNTs/FET with the three Hg(II) concentrations (100 pM, 10 nM and 1 μM) at V_{DS}=0.02 V and V_G=0 V. Each data point is an average of measurements from 5 independent biosensors.

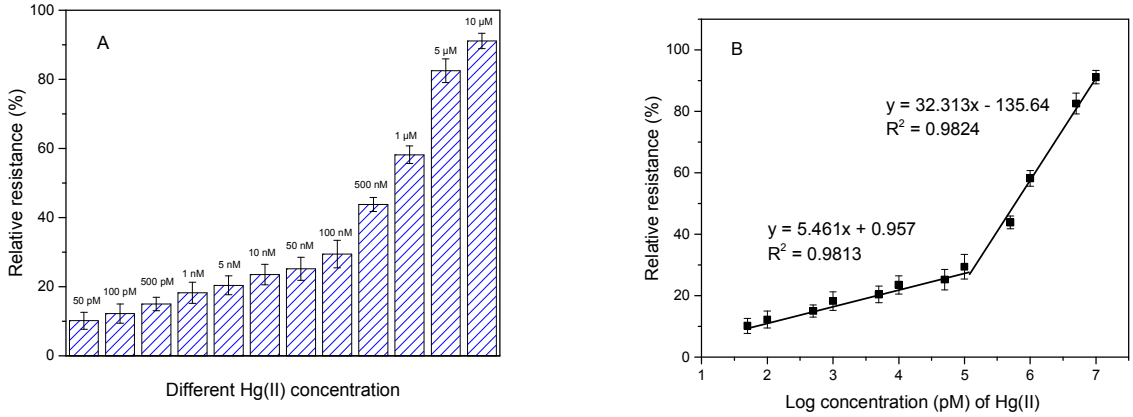

Figure 6. . (A) Relative resistance change after Hg-DPR/SWNTs/FET exposed to different Hg(II) concentrations (50 pM, 100 pM, 500 pM, 1 nM, 5 nM,10 nM,50 nM,100 nM ,500 nM ,1 μM, 5 μM and 10 μM); (B) Linear regression of relative resistance vs. the logarithm of Hg(II) concentration. The error bars indicate standard deviations from five biosensors.

Table 1. Comparison of the parameters of other published sensors using for Hg(II) determination

Sensor	Method	Linear ranges (nM)	Limit of Detection (nM)	Time (min)	Reference

MoS_2/FET	IV	1-1000	0.03	10	[38]
citrate-capped AuNPs	UV-vis	5-1000	2.9	5	[39]
G-quadruplex	UV–visible absorption	20-500	20	-	[40]
TGA-AuN/Rgo/FET	IV	25-14200	25	0.17	[41]
hemin/G-quadruplex	UV–vis	0.05-20	0.01	-	[42]
DNAzymes	fluorescence	20-500	2.4	5	[43]
Hg-DPR/SWNTs/FET	IV	0.05-100 and 100-10000	0.01	3	This work

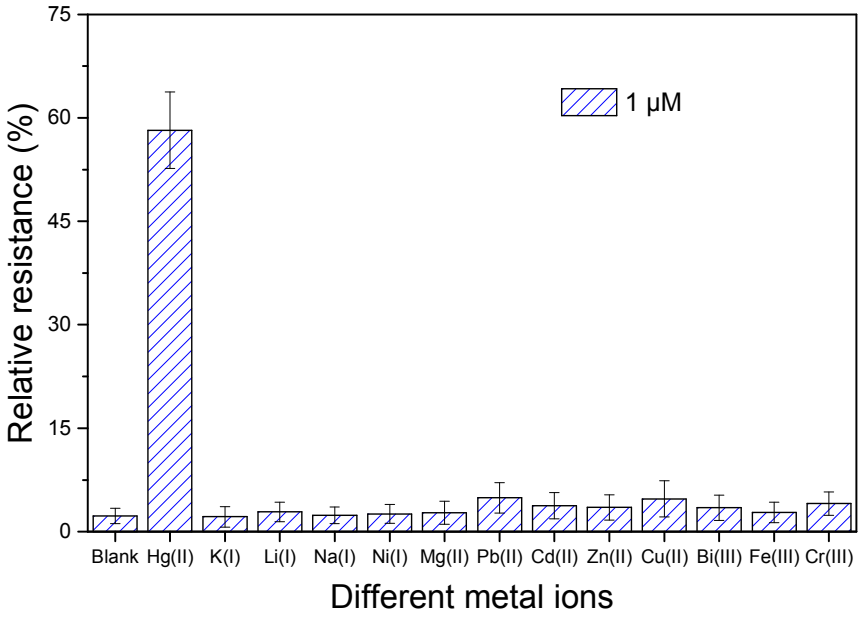

Figure 7. Relative resistance of Hg-DPR/SWNTs/FET before and after adding different 1 μM metal ions. The error bars indicate standard deviations from five biosensors.

Table 2 Determination of Hg(II) in water and soil samples using the Hg-DPR/SWNTs/FET.

Sample	Adding Hg(II)	Hg-DPR/SWNTs/FET	AFS	Recovery (%)
		Detection Concentration	Detection Concentration	
water 1	-	23.28±2.52 nM	25.31 nM	91.98
	50 nM	78.34±5.34nM	-	104.02
water 2	-	18.34± 2.87 nM	17.65 nM	103.90
	50 nM	69.34±4.13 nM	-	102.49
Soil 1	-	1.88±0.22 μM	1.95 μM	96.41
	2 μM	3.96±0.52 μM	-	100.3
Soil 2	-	2.31±0.48 μM	2.14 μM	107.94
	2 μM	4.49±0.47 μM	-	108.45

※The error bars indicate standard deviations from four biosensors.

For TOC